Conference Paper

"Profile PIV" - more than just an optical hotwire: new potentials of PIV in boundary layer research

Author(s):
Willert, Christian E.

Publication Date:
2018-10-05

Permanent Link:

https://doi.org/10.3929/ethz-b-000280170 →

"PROFILE PIV" - MORE THAN JUST AN OPTICAL HOTWIRE NEW POTENTIALS OF PIV IN BOUNDARY LAYER RESEARCH

Christian E. WILLERT [1,a]

[1]Institute of Propulsion Technology, Deutsches Zentrum für Luft- und Raumfahrt (DLR), 51170 Köln, Germany
[a] Corresponding author: Tel.: +49 2203 6012308; Email: chris.willert@dlr.de

KEYWORDS:
Main subjects: flow visualization, image-based velocimetry
Fluid: turbulent boundary layer, validation data, wall shear stress
Visualization method(s): particle image velocimetry, particle tracking velocimetry
Other keywords: laser diagnostics, turbulence

***ABSTRACT**: The article provides an overview of the development, implementation and application of a recently developed variant of the particle image velocimetry (PIV) technique. The so-called "profile-PIV" approach utilizes high aspect ratio image formats to capture velocity data along narrow strips rather than providing the nearly square flow maps characteristic of PIV. Using a high-speed camera, the smaller image format allows the image capture at frame rates up to and beyond 100 kHz such that converged velocity statistics become feasible when using sample counts of similar magnitude. The narrow field of view permits a proportional reduction of the laser power required for particle illumination. For medium speed air flows (U < 10 m/s) a CW laser is suitable, whereas pulsed diode lasers are required at higher velocities. When operated with high image magnification near 1:1, the technique provides access to near-wall velocity statistics of boundary layer flows, in particular, allowing the recovery of the mean and unsteady wall shear stress, even at higher shear Reynolds numbers, provided the viscous scales can still be resolved by the imager's pixels. The potential of the "profile-PIV" technique is demonstrated with examples from a variety of recent applications is given, mainly in the area of turbulent boundary layer investigation.*

1. Introduction

This manuscript is largely based on the material presented during the *ISFV Asanuma Award* lecture given by the author during the *18th International Symposium of Flow Visualization* held in Zurich, Switzerland, in June 2018. The intention of the article is to mainly provide an overview of an implementation of the PIV technique developed and applied by the author in the past five years. As such, only the underlying concepts of the approach and highlights from a variety of recent applications are presented herein. Further details on the presented material can be found in corresponding recent publications that are referenced throughout the text. The technique as such is described in [17].

Since its introduction in the mid 1980's, the particle image velocimetry (PIV) technique has matured to become the method of choice for fluid flow measurement in both fundamental and applied research. In its basic implementation, PIV provides two-dimensional snap-shots of the fluid flow under investigation using a double-frame image capture of small tracer particles illuminated by a light sheet plane, typically by means of a double-pulsed laser. Details on the technique's implementation and multifold applications can be found in numerous publications and are beyond the scope of this article (see e.g. [1][10]).

The intention of the present contribution is to introduce a variant of the PIV technique that is specifically catered for the reliable measurement of turbulence statistics [17]. This type of data is of great importance for the validation of computational fluid dynamics (CFD), in particular, to assess the

performance of turbulence models utilized by the Reynolds-averaged Navier-Stokes (RANS) simulations and large eddy simulation (LES) methods. Due to the large range of scales present in most technical flows, in particular turbomachinery flows, both RANS and LES will continue to play a dominant role in the aero-thermal design process for the years to come. In this context the large variety of flow phenomena present in turbomachinery flows frequently cannot be adequately captured by existing simulation methods, requiring further improvement of the underlying turbulence models.
To illustrate the demand for validation data, Fig. 1, left, provides an overview of the multitude of flow phenomena present in a compressor cascade as visualized by oil flow surface visualization. Toward the trailing edge, the suction side of the blade exhibits a large separation zone that is associated with blockage and reduced performance of the compressor stage. Also visible is the foot print of transition bubble, downstream of which the boundary layer flow is turbulent. As shown in Fig. 1, right, most of these features are in fact captured using the in-house RANS based CFD solver TRACE [3]. However, the size and strength of the separation zone is underestimated, which is mainly due to the deficiencies of the underlying turbulence models. On this background detailed 3D-PIV measurements were performed with the aim of mapping out the size and strength of the recirculation zone. For the measurement, tomographic PIV, a photogrammetric implementation of the PIV technique was selected, as it has the potential of providing unsteady, volume-resolved velocity data [6][8]. The complexity of the instrumentation required for tomographic PIV can be partially seen in Fig. 2, left, as it requires the precise alignment of a multitude of cameras onto a given volume of interest through the thick optical windows of the compressor cascade. Fig. 2, right, presents the averaged flow field acquired in the separation zone by means of tomographic PIV. The data set is the result of careful tuning of laser illumination, imaging parameters and particle seeding density to achieve adequate data without running the risks of contaminating the windows with particle seeding that in turn would lead to signal deterioration or even signal loss. Also the increased depth resolution could only be achieved by reducing the in-plane resolution as the maximum achievable information density is limited by the actual size of the image sensor. As a consequence, the spatial resolution of the acquired 3D data will be lower than for planar (2D) data.

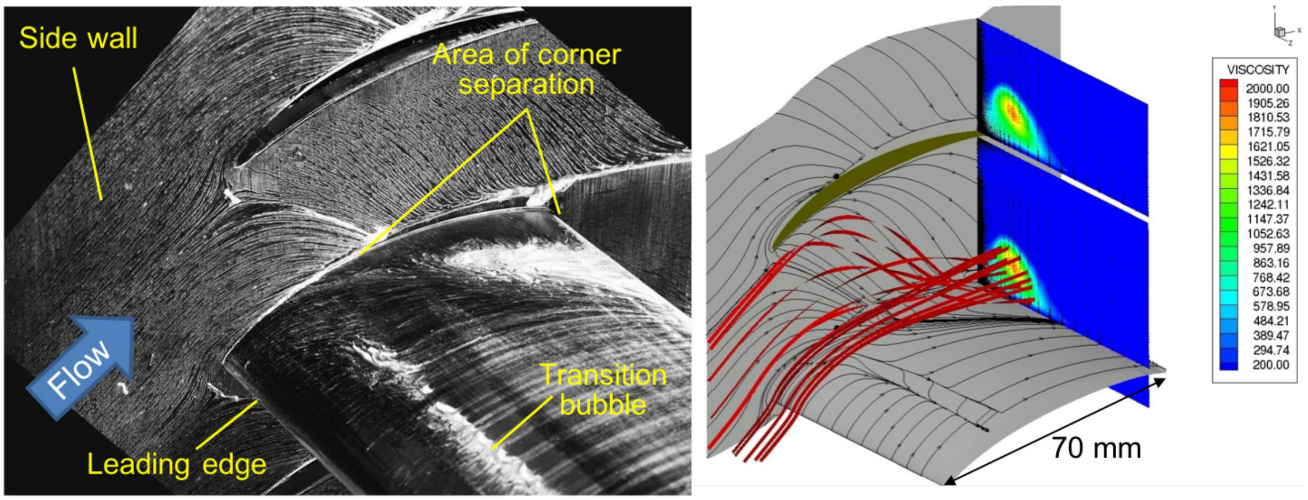

Fig. 1: Left: Surface flow visualization in a turbomachinery compressor cascade showing various flow phenomena; right: matching RANS simulation result for similar operating conditions, color represents eddy viscosity (inlet Ma = 0.6) [7]

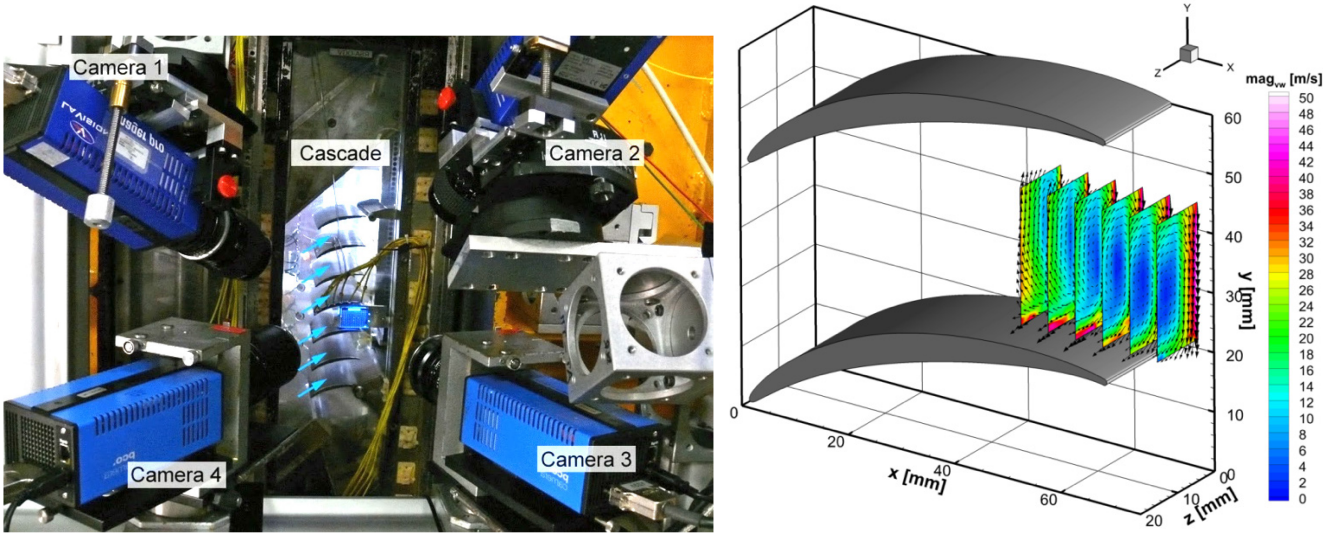

Fig. 2: Volumetric measurement of the separation zone by tomographic PIV (J. Klinner, 2017 [8])

The previous example illustrates the potential of 3D PIV for the analysis of complex turbomachinery flows. Along with the more wide-spread conventional 2D PIV, one of the primary strengths of PIV is its capability of providing snap shots of the flow field thereby giving insights to flow topology such as vortical structures. However, due to the large amount of data necessary, PIV is typically less suited for the generation of statistics data. Aside from the high data volume involved, the time required for PIV analysis can be considerable to prohibitive. At the same time, the data required for the validation of numerical methods generally does not make use of the unsteady velocity data provided by PIV but rather relies on mean values and higher order statistics calculated from the snap-shot data. The demand for converged velocity statistics for validation use motivated the development of a PIV implementation that fulfils primarily this purpose and is subject of the remainder of this article.

2. Development and implementation of the “Profile-PIV” Technique

The “profile-PIV” measurement approach originated as a feasibility study conducted in 2013 at the Institute of Propulsion Technology and was aimed at assessing the potential use of comparatively cheap CW lasers for high speed imaging of low- to medium speed flows, rather than using costly high-speed lasers, which, depending on their output power, can exceed 100,000 US$ in cost. The underlying philosophy of the investigation was the acquisition of narrow strips of velocity data rather the near square aspect ratio imaging of planar velocity fields that are typical of conventional PIV imaging [17]. The use of high aspect ratio imaging of the “profile-PIV” technique inherently has two clear advantages: On the illumination side, the available laser light can be bundled into a narrow strip of a few millimeters width, thereby providing the luminous flux required to sufficiently illuminate the particles such that they can be imaged by the camera’s sensor. This allows the use of (cheaper) lasers with proportionally less output power. On the imaging side, the high aspect ratio allows the camera to be operated at significantly increased frame rates, up into the 100 kHz range and more. Beyond this, the smaller images allowed a proportional increase of the number of images that can be captured as a single sequence given the limited size of streaming memory of today’s high-speed cameras. With this high aspect ratio sensor configuration sequence lengths beyond 100,000 images are easily feasible.

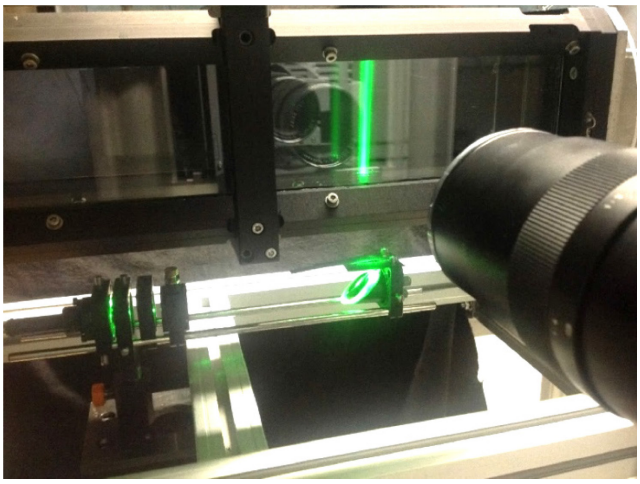

Fig. 3: Initial imaging setup of the "profile PIV" technique on a small wind tunnel in May 2013

A photograph of the initial imaging setup of the profile-PIV technique is shown in Fig. 3, where it is applied to small wind tunnel of 76×76 mm^2 cross section and bulk velocity of 4 m/s. The ~5 mm wide light sheet was formed from the beam of a 5W continuous wave (CW), frequency doubled Nd:YAG laser (Coherent Verdi V5, 532 nm) by a pair of cylindrical lenses in telescope arrangement. A spherical lens focused the light sheet to abont 300 µm thickness within the observed domain. On the imaging end, a $f = 100$ mm macro-lens (Zeiss Makro Planar, 100mm/f#2) imaged the illuminated particles onto the sensor of a high-speed camera (Photron SA5), which has an maximum frame rate of 7 kHz at full resolution of 1024×1024 pixel. Reduced to field of view of 1024(H)×256(W) pixels, frame rate exceeding 25 kHz are possible. Seeding was provided by ~1µm paraffin oil droplets from a Laskin principle seeder with attached impactor to separate out larger droplets.

A sample image acquired with the described setup is provided in Fig. 4. The camera frame rate was set at 20 kHz along with an electronic shutter of 20 µs to prevent excessive streaking of the continuously illuminated particles. Near the bottom of the image the dark line is created by light scattered on the glass surface[1] with mirrored particle images visible below. The image magnification was set at unity resulting in 20 µm pixels in physical space.

Fig. 4, right, shows a single velocity vector field of the continuous image sequence obtained using a conventional two-frame, cross-correlation based PIV processing algorithm using sample sizes of 64(W) ×8(H) pixels (1.28×0.16 mm^2). Near the upper end of the image the velocity of the developing channel flow boundary layer reaches the bulk velocity of 4 m/s with corresponding particle image displacements of 8 pixels between successive recordings. The color-coding in Fig. 4, right, represents estimates of the local out-of-plane vorticity obtained by finite differencing applied to the velocity data.

For the strongly statistics driven "profile PIV" technique the result provided in Fig. 4, right, is only an intermediate result. Typical processing of the image sequence involves the extraction of single column of velocity vector and associated differentials from each of the image pairs to arrive at a continuously evolving velocity profile, in the present case, oriented normal to the wall. A subset of such a record (from a different experiment) consisting of about 400 samples is shown in Fig. 5 for the streamwise and wall-normal velocity components. This type of data is the basis for further post-processing to obtain, for instance, the mean velocity profile, higher-order moments, 2-point correlations and spectra.

[1] By properly cleaning the surface the light scattering at the air/glass interface can be nearly eliminated.

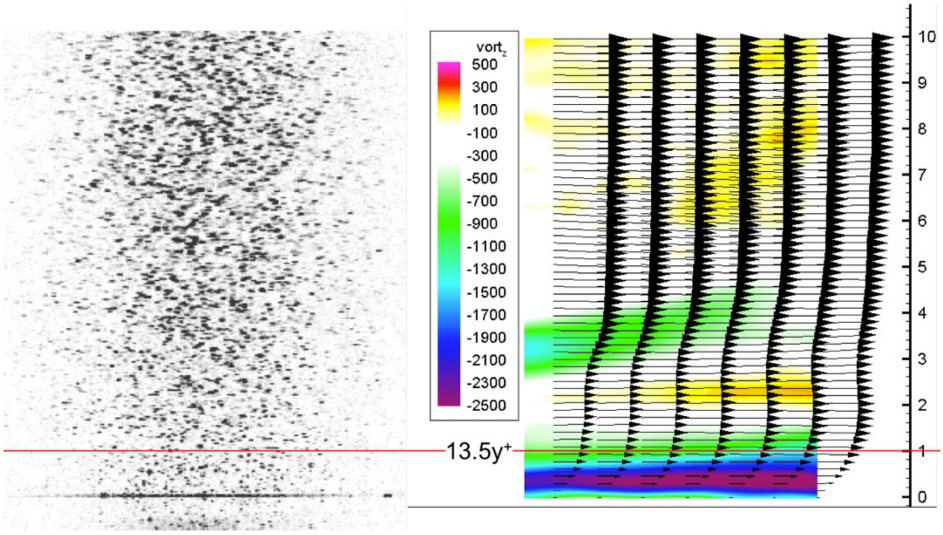

Fig. 4: Single image of sequence acquired at 20 kHz (left) shown with inverted lookup table, image width is 256 pixel; right: single 2D-2C PIV data set obtained from sequence. Color coding represents out-of-plane vorticity.

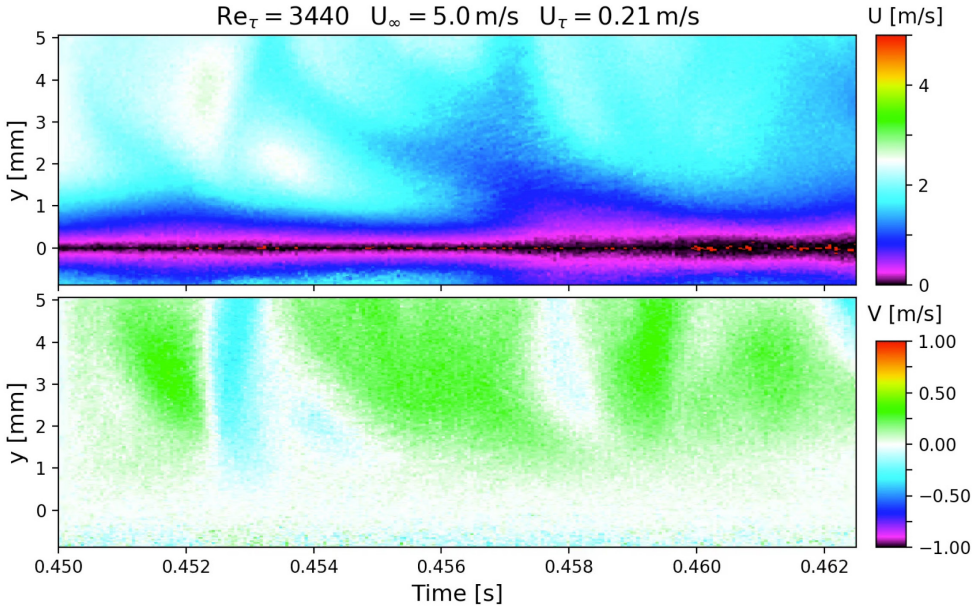

Fig. 5: Portion (400 samples) of time-evolution of the two velocity components along a wall-normal line. Y=0 represents the wall. Velocity data below the wall.

For the given flow conditions the PIV image provided Fig. 4 has an effective magnification of about 3.7 pixels per viscous unit, the ratio of kinematic viscosity and shearing velocity ν/u_τ. The sample height of 8 pixels chosen for PIV processing therefore has a height of about two viscous units which corresponds to the Kolmogorov length scale at the wall.

The rather slow, wall parallel motion of particles near the wall can be followed over many image samples. In fact, by compiling wall-parallel lines of pixels for a fixed wall distance into a composite image, particle streak images can be generated such as shown in Fig. 6, left. The slope of the particle tracks within these x-t diagrams is a measure of the particle's instantaneous velocity. With increased distance from the wall the slope and with it the velocity increases. Quantitative information on the instantaneous particle velocity can be recovered using, for instance, cross-correlation processing of

adjacent lines of image data. To illustrate this, Fig. 6, right, shows the temporal evolution of the mean particle motion for different wall distances retrieved from the particle streak images shown on the left. The velocity data shows a clear linear coherence across the viscous sublayer which is to be expected within the viscous layer. Here it should be noted that the velocity represents the mean particle velocity across the image width (256 pixels or 2.1 mm). By reducing the length of the sample used for the correlation analysis or by tracking the particles individually the spatial averaging can be reduced proprotionally.

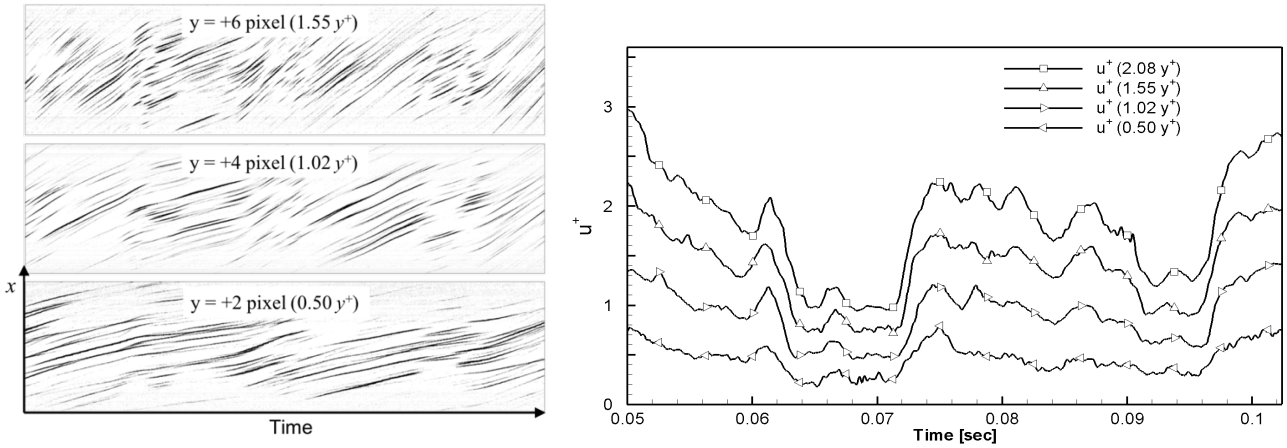

Fig. 6: Left: Streak images obtained at different wall distances by extracting wall parallel lines from each image of a sequence (images represent 1024 time steps of O(100,000) samples. Right: corresponding time record of the evolving streamwise velocity, normalized by the mean shear velocity u_τ obtained by 1-D cross-correlation analysis of the streak images (from [17]).

The linear behavior of the near wall velocity in viscous sublayer can be exploited to recover the velocity gradient at the wall or wall shear rate using linear least squares fitting. With this value the stream-wise wall shear stress $\tau_{w,x}$ can be estimated directly:

$$\tau_{w,x} = \mu \left.\frac{\partial u}{\partial y}\right|_{y=0} \tag{1}$$

The mean wall shear rate $\partial u/\partial y$ is related to the mean friction velocity u_τ and required to estimate the viscous unit ν/u_τ of the boundary layer flow under investigation:

$$u_\tau = \sqrt{\frac{\tau_{w,x}}{\rho}} = \sqrt{\nu \left.\frac{\partial u}{\partial y}\right|_{y=0}} \tag{2}$$

It should be noted that estimation of the wall shear rate from the particle image data can essentially considered to be a calibration-free approach, as only the laser pulse separation needs to be known; any spatial scaling related to camera magnification cancels out. Thereby, this approach holds the potential of accurately measuring the wall shear stress, both in the mean and unsteady, provided sufficient resolution of the viscous sublayer and sufficient seeding with particles of low Stokes number (e.g. good response to dynamics of the flow).

Fig. 7, left, provides an example of the estimation of the mean wall shear rate from the mean displacement determined for different wall distances. The blue symbols indicate the values used for the linear fit. The departure from linearity near the wall can be attributed to laser scatter on the wall resulting in a bias toward zero displacements in the absence of particle images. At greater wall distances the departure from linearity is indicative of transition into the buffer layer. For instance, at a wall distance of $y=3^+$ (viscous units), the departure from linearity already amounts to ~1% increasing to

~2% at y=4$^+$. Therefore only displacement estimates below y=3$^+$ should be used for the estimation of the wall shear rate.

Beyond the estimates of the mean shear rate and with it the mean stream-wise shear stress, the unsteady velocity data obtained from the streak images lends itself to provide the unsteady wall shear stress $\tau'_{w,x}$, which always has been a challenging task in experimental fluid mechanics. These values can be estimated by performing linear least squares fitting just as for the mean wall shear rate and can be further used to obtain information on the statistics and frequency spectrum of the wall shear stress. As an example, Fig. 7, middle and right, shows the probability density distribution (PDF) of the wall shear stress of a turbulent boundary layer of Re_θ = 8120 and represents 100,000 independent samples (acquired at 200 Hz). The log-linear representation indicates the presence of extreme wall shear rates in excess of 6 standard deviations from the mean with probabilities well below 10^{-3}. Also, negative wall shear stress events are suggested by the data points located to the left of $\tau'_{w,x}$, = 0. These are associated with rarely occurring flow reversal events [19].

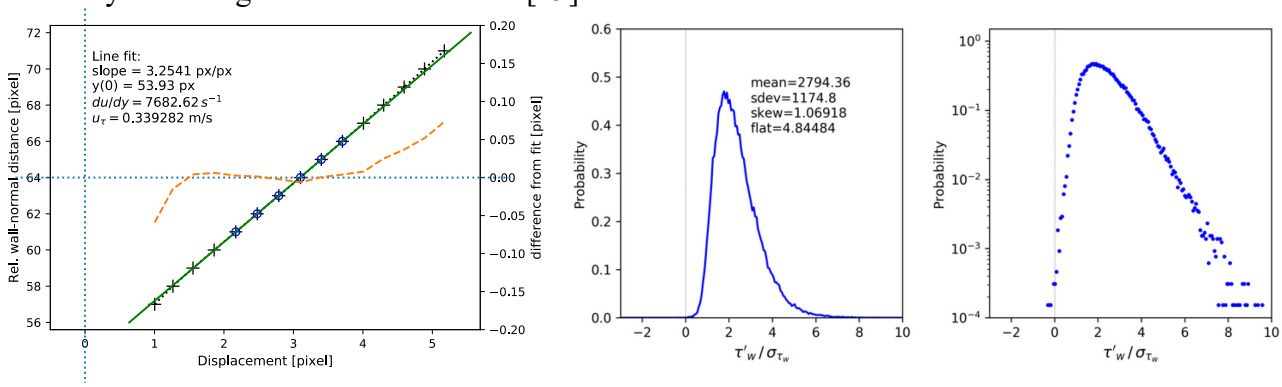

Fig. 7: retrieval of the near-wall velocity gradient du/dy from the velocity profile using linear least squares fitting to estimate the friction velocity u_τ ; right: PDF's of the unsteady wall shear rate for a single image sequence both in linear and log-linear scaling.

3. Recent applications using the "profile PIV" technique

Since its initial lab-scale implementation in 2013 the PIV-based profile measurement technique has been applied in numerous projects, in particular involving investigations of turbulent boundary layers. The following sections give a brief overview of these. The variety of applications encountered thus far is illustrated in Fig. 8. Several turbulent boundary layer measurements were performed in the 1m and 2m wind tunnels of the DLR Institute of Aerodynamics and Flow Technology with Reynolds numbers ranging up to Re_θ = 10,000 (U_∞ = 15 m/s) [13]. Within the EuHIT project, measurements were first performed in an adverse pressure gradient (APG) turbulent boundary layer, described in the following section, and later on in a turbulent pipe at shear Reynolds numbers reaching Re = 40,000 [18]. A joint campaign between ONERA and DLR in a water tunnel investigated the flow around a cube interacting with laminar and turbulent boundary layers (Fig. 8d). Here the "profile-PIV" provided detailed boundary layer characteristics at several positions, completing an extensive data base involving both global 2C-2D PIV as well as time-resolved 3D PIV [12].

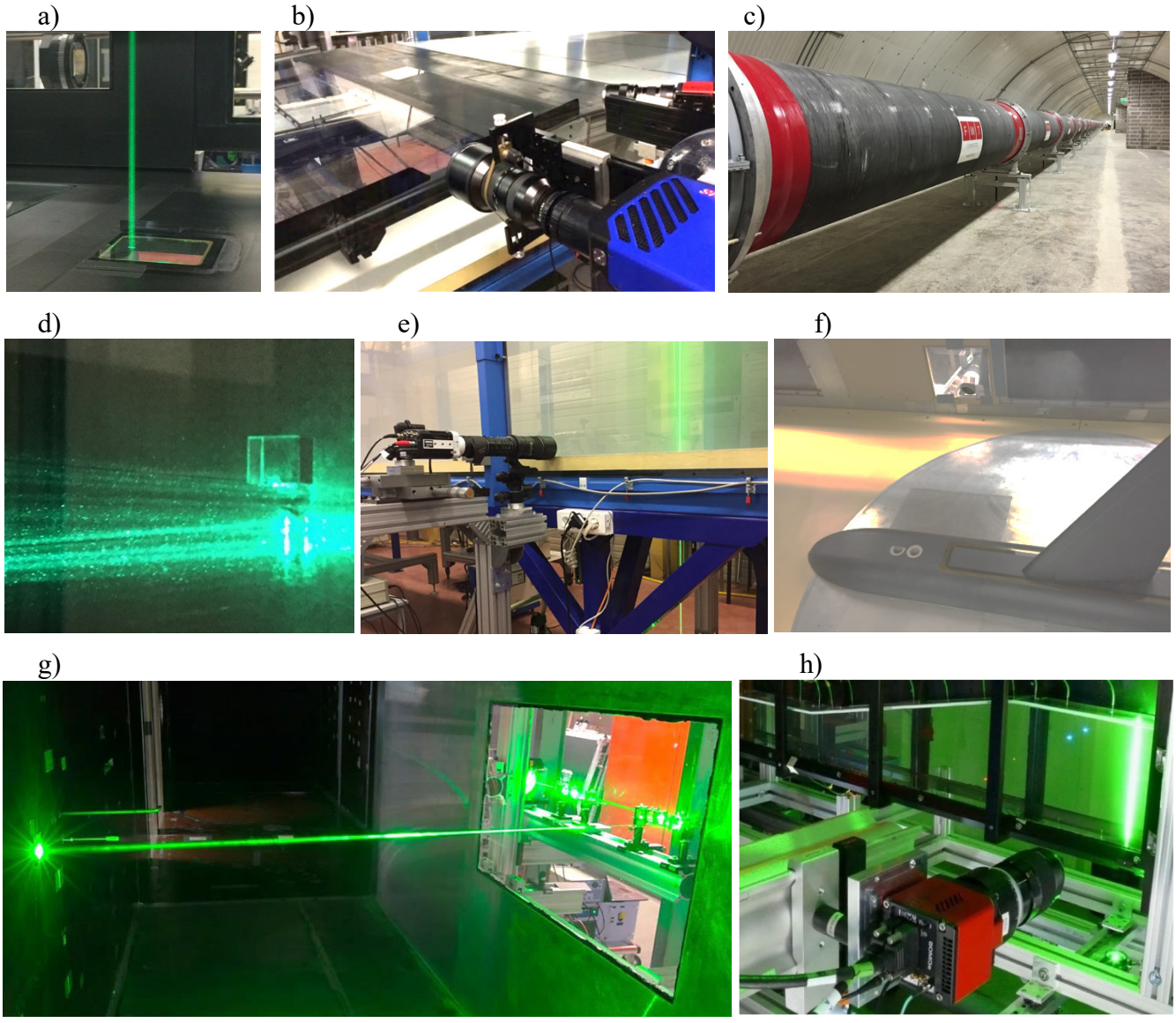

Fig. 8: Photographs of experimental setups in which the profile-PIV technique was used: a) 1 m wind tunnel of DLR Göttingen [13], b) EuHIT Project "Large Scale Structure" at LMFL, Lille [4], c) EuHIT project "HoloPipe" at CICLoPE of Univ. Bologna [18], d) DLR-ONERA Common Research Project "CUBE" [12], e) near wall flow statistics at LMFL, f) wing-body junction flow at the California Institute of Technology, g) APG investigation within DLR project "VicToria" at UniBW Munich [14], h) diffusor channel of DLR project VicToria" at DLR Köln.

3.1. Measurements of high Reynolds number turbulent boundary layers

3.1.1. EuHIT Project Large Scale Structure

The "profile-PIV" technique found its first application outside of DLR at the boundary layer windtunel of the Laboratoire de Mecanique des Fluides des Lille (LMFL) during the EuHIT project "Large Scale

Structures"[2]. The project's aim was to combine several different PIV setups in order to obtain detailed measurements of the developing boundary layer subjected to an adverse pressure gradient. The wind tunnel with installed ramp model is shown in the photograph of Fig. 9, left. The model first accelerates the flow over a distance of about 3.5 m before transitioning to decelerating ramp adverse pressure gradient Aside from large field PIV imaging involving 16 synchronized sCMOS cameras placed side-by-side, the "profile-PIV" technique was used to obtain reliable estimates of the wall shear stress and with it the friction velocity. Beyond this the technique extended the velocity profiles provided by the large field imaging down into the viscous sublayer with spatial resolutions in the order of a single wall unit.

Fig. 9, right shows the imaging setup in the APG area using a high-speed CMOS camera (PCO Dimax-S4) with 11 µm sized pixels. A lens of 300 mm focal length (Zeiss Apo-Tessar 300/2.8) enabled imaging at the wind tunnel's centerline with a magnification of m=0.44 (25 µm/pixel) at a working distance near 1.05m. By reducing the field of view of the camera down to 178(W) × 288(H) the 36 GB of the camera's memory could provide sequence lengths exceeding 500,000 images at 6.7 kHz (sequence duration 75 s). Particle illumination was provided by a pair "low cost" CW lasers with combined power of ~10W at 520 nm (Kvant Laser, SK) whose beams were overlapped into a common light sheet of ~300 µm thickness. Seeding was provided by a smoke generator operating with a water glycol mixture. The long image sequences provided reliable turbulence statistics such as shown in Fig. 10. A comprehensive compilation of the experiment and acquired data is available in [4].

Fig. 9: Left: Windtunnel of LMFL in Lille with ramp model installed; right: highspeed camera with 300mm lens for high magnification imaging [4].

[2] EuHIT (European High-performance Infrastructures in Turbulence) was an EU-FP7 funded project providing transnational access to large scale turbulence test facilities infrastructure. See www.euhit.org for details.

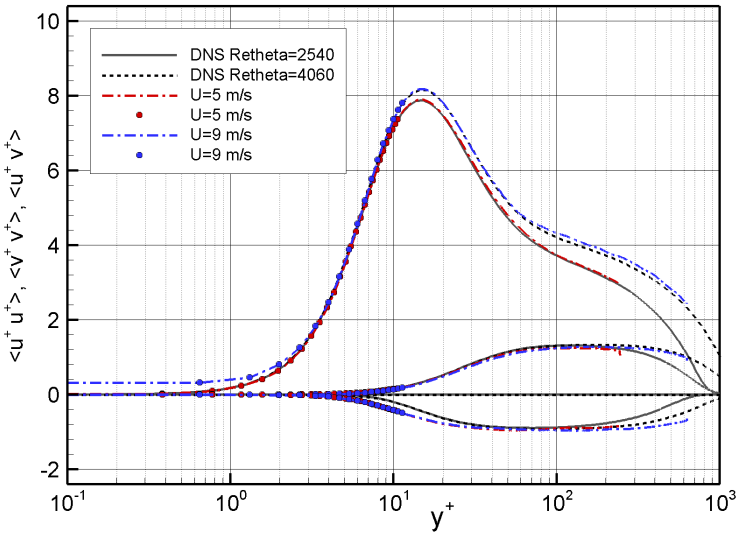

Fig. 10: Variances and co-variances scaled with inner variables obtained upstream of the model in comparison with DNS data for similar Reynolds numbers [4].

3.1.2. Study of wall shear stress statistics

In the course of the analysis of the long image sequences acquired during the EuHIT campaign at LMFL seemingly unusual flow reversal events could be observed, that upon closer inspection were found to be self-similar and present at all measurement locations. Previous DNS simulations and, more recently, measurement data already documented the existence of these short lived features that are associated with localized negative wall shear stress.

To study the flow reversal phenomena in more detail a second measurement campaign was performed at LMFL in November 2017, in an effort to provide reliable data at the same operating conditions at roughly twice the magnification. Here a 300mm lens (Nikon Micro-Nikkor 300/4) coupled with a 2× teleconverter (Nikon TC2.0) resulted in a magnification of $m = 0.85$ with an effective pixel size of 11.7 µm in object space (Fig. 11, left). At the highest velocity ($U_\infty = 9$m/s) this magnification provides about 4 pixels per viscous unit. The field of view was approximately 2.5×6.0mm^2 in size and imaged by a high-camera with 10 µm pixel pitch and 12GB of RAM (Vision Research, Phantom Miro 341). Up to 42 sequences of 70,000-93,000 images each were acquired for each condition. Just as in previous measurement campaign a fog generator operating with a water glycol mixture provided the necessary seeding of 1-2 µm droplets. Due to the high magnification a very high seeding density of approximately 3000 droplets per mm^3 was necessary to allow processing with sample heights close to or smaller than the Kolmogorov length scale. A representative raw image acquired in the APG region at $U_\infty = 5$ m/s is shown in Fig. 11, middle, with the red dashed line indicating the height of the viscous sublayer ($y = 5^+$).

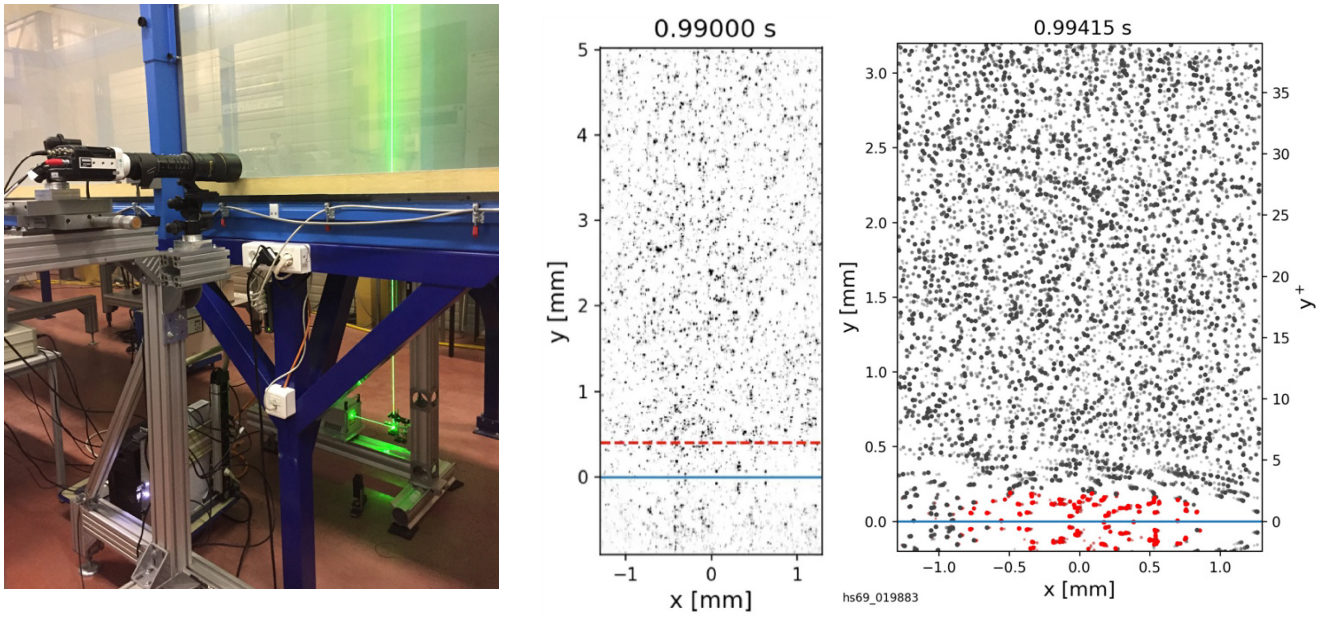

Fig. 11: left: high-magnification imaging using a lens of 600mm effective focal length; middle raw image from the APG region with background subtracted; right: PTV result comprised of 5 frames with a flow reversal area color-coded in red. Viscous scaling is given on the right axis.

The combination of high seeding density and high frame rates allows the image data to be analyzed by advanced, multiple frame particle tracking (PTV), for which a result is shown Fig. 11, right. The particle detection scheme is similar to the iterative particle reconstruction (IPR) [16] used in the 3-D shake-the-box algorithm (STB) developed by Schanz et al. [11] for 3-D tracking of particles. The particle tracks highlighted in red in the PTV image of Fig. 11, right, are associated with a motion in upstream direction and represent a single flow reversal event which have a probability of occurrence on the order of 10^{-4}.

The same flow reversal event is also visible in the time resolved velocity profile shown in Fig. 12, top, indicated as a red patch at y=0 height at t = 0.497 s.

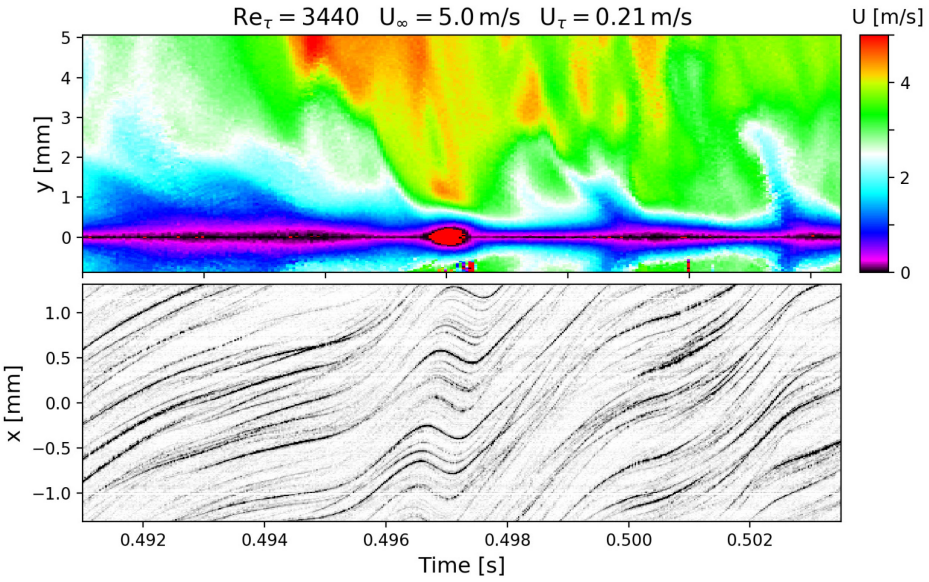

Fig. 12: Time trace of the streamwise velocity component (top) and corresponding particle streak image in the viscous sublayer about $1.0y^+$ from the wall. The red spot near the center indicates a flow reversal event.

As described in Sec. 2, the particle streak images can be used for the estimation of the unsteady wall shear stress. Given large number of samples acquired in the course of the experiments at LMFL it is possible to compile PDF's of the wall shear stress such as shown in Fig. 13. Most of literature to date typically provides plots in linear scaling as on the left of Fig. 13 and only recently data has become available to warrant a log-linear presentation. In the present case a weak influence of Reynolds number can be observed, indicating a higher probability for extreme shear stress events with increased Re. This is consistent with recent DNS data [5][9]. The probability of negative shear stress and corresponding flow reversal events does not seem to significantly affected by the change of Reynolds number [20].
For the investigated high Reynolds number flows estimates of the rms value of the wall shear stress are also accessible. For the studied ZPG boundary layer flows the data is summarized in Fig. 14, left, whereas the right plot presents data for turbulent pipe flow at shear Reynolds numbers up to Re_τ = 40,000. To the author's knowledge this data to date has not been available for Reynolds numbers in this range. In the plots the dashed line indicates a correlation originally formulated by Alfredsson et al. [2] and further refined by Örlü & Schlatter [9].

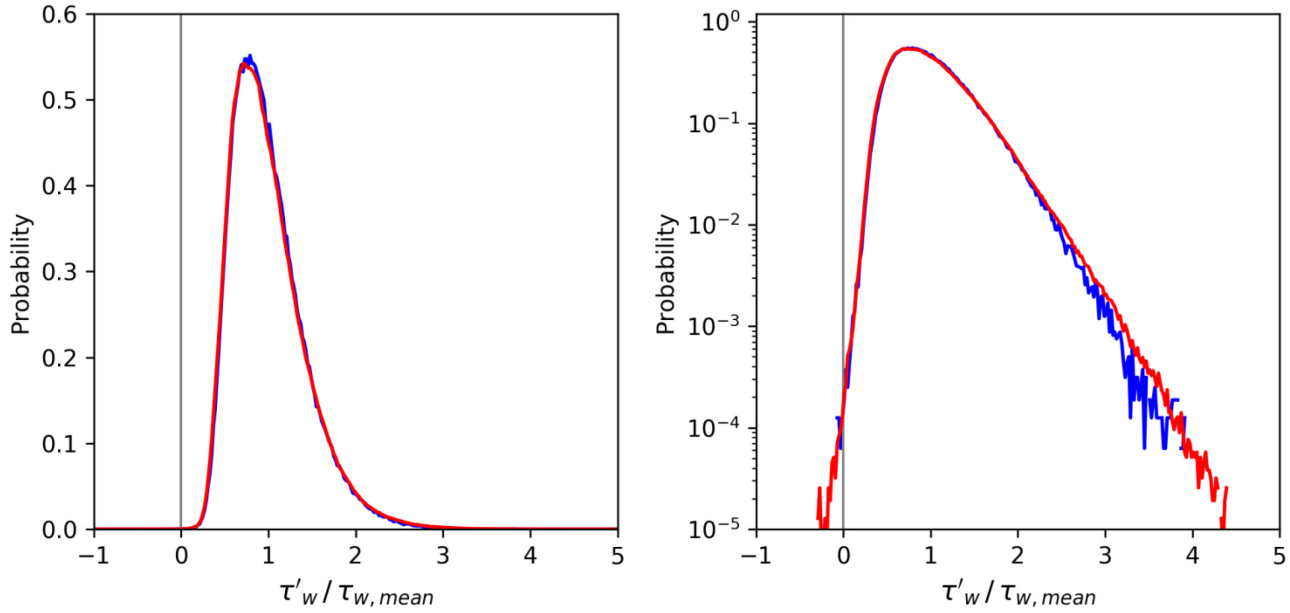

Fig. 13: Measured PDFs of the unsteady wall shear stress for Re_θ = 8120 (blue) and Re_θ = 18360 (red)

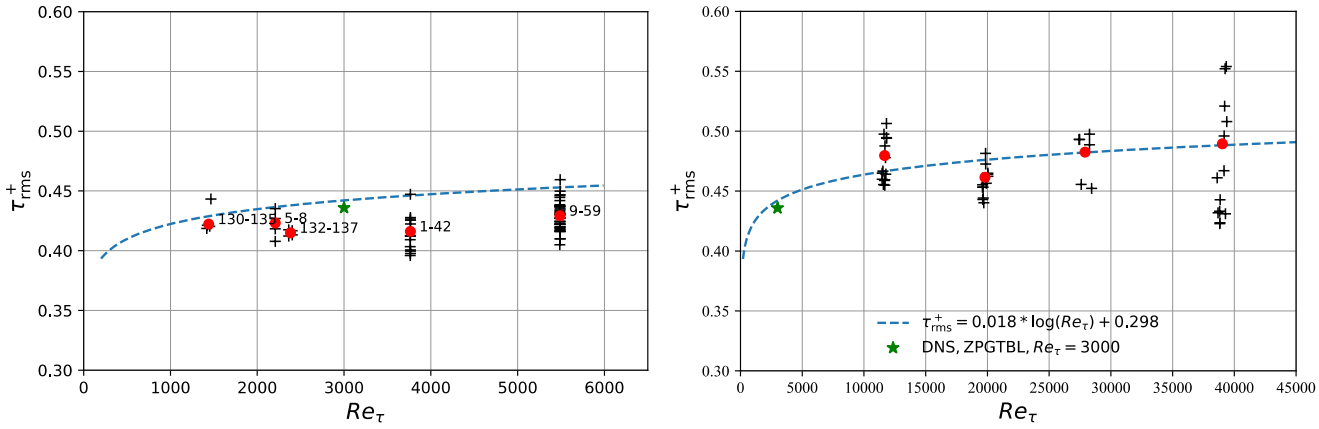

Fig. 14: Wall shear stress fluctuation estimates obtained from ZPG turbulent boundary layer (left) and turbulent pipe flow (right); DNS data marked with green star provided by J.P. Laval, LMFL [15]

3.1.3. Boundary layer measurements at higher flow speeds

With increasing bulk velocity the wall-shear rates increase while the viscous scales reduce. This implies that the magnification needs to be increased to resolve the viscous scales which in turn requires a significantly higher camera frame to achieve similar particle image displacements on the sensor. One such application is shown in Fig. 8(g) for a windtunnel boundary layer investigation subjected to an adverse gradient [14]. At the given measurement location the aim was to provide flow statistics upstream of an adverse pressure gradient ramp with strong flow deceleration. To overcome a working distance of 1m a 400mm lens (Nikon Mikro-Nikkor 200/4 with TC2.0 teleconverter) was used, providing a magnification of m=0.46. The highspeed camera (Photron SA-X2, 20 µm pixel pitch) was operated at up to 50 kHz with a field of view of 6.5×44 mm^2 (152×1024 pixels). The acquired image data was processed with sampling windows of 48×6 pixels or 155 x^+ × 20 y^+ in viscous units ($\nu/u_\tau \approx$ 13.5 µm). Plots of the mean and variances for two different flow conditions are provided in Fig. 15. While mean streamwise velocity follows the expected profile down to the buffer layer, the viscous sublayer is not resolved. When compared to DNS data considerable differences can be seen for the variances where the inner peak at $y = 15^+$ is not being resolved. Also the variance of the wall-normal component $\langle v'v' \rangle^+$ is significantly underestimated. This can be explained by the rather large sampling window which acts as a low-pass filter on the velocity field; its height (~20 y^+) is about four times larger than the viscous sublayer – as indicated by the beige shaded region in Fig. 15.

The ideal way of overcoming this resolution issue is to increase the magnification, preferably to have several pixels per viscous unit using a camera with smaller pixels and/or a longer focal length lens. As the experiment could not be repeated, the existing data was reprocessed using a particle tracking scheme that allows, in principle, the assignment of velocity vectors to each detected particle image. In the present case, the recently developed 3-D "shake-the-box" particle tracking scheme, STB, [11] was modified for the analysis of two-component PIV images. With the 2D-STB processing scheme an average of about 2000 particles could by tracked over multiple frames and provided reliable estimates of their respective velocities. Flow statistics were then obtained using bin-averaging with a bin height of 0.25 pixels (≈1y^+), with each bin containing on the order of 100,000 samples. Compared to the PIV result the spatial resolution is effectively increased by at least an order of magnitude (0.25 pixels vs. 6 pixels). As shown in Fig. 16 the mean and variances now closely match the expected profiles of a

typical ZPG boundary layer. Deviations near the wall are caused from erroneous particle tracking caused by laser flare on the glass surface and the influence of mirrored particle images.

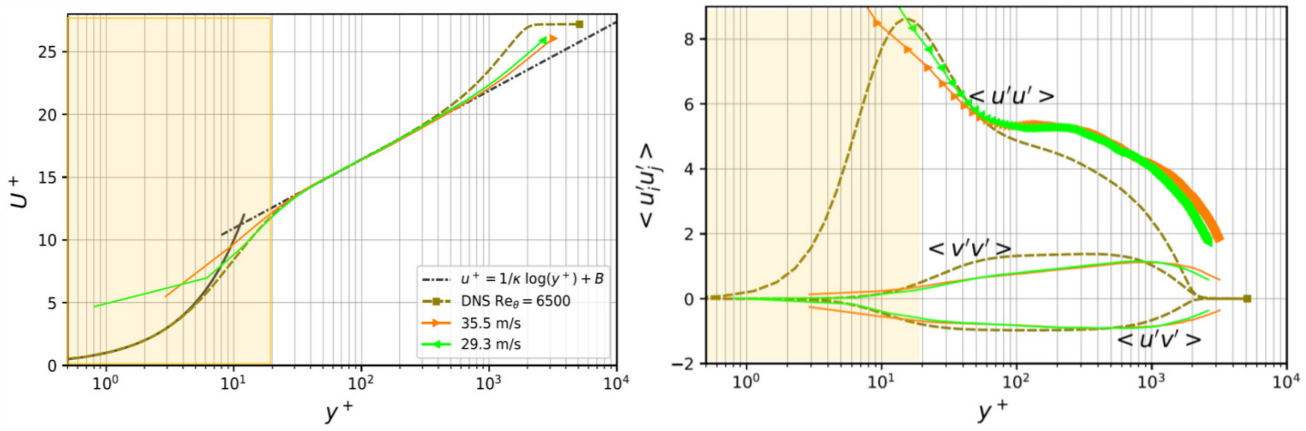

Fig. 15: Measured velocity profile (left) and associated variances (right) with inner (viscous) scaling of a boundary layer flow at free stream velocities of 29.3 and 35.5 m/s. The beige shaded areas indicates the height of the PIV sampling window (6 pixels), from [14].

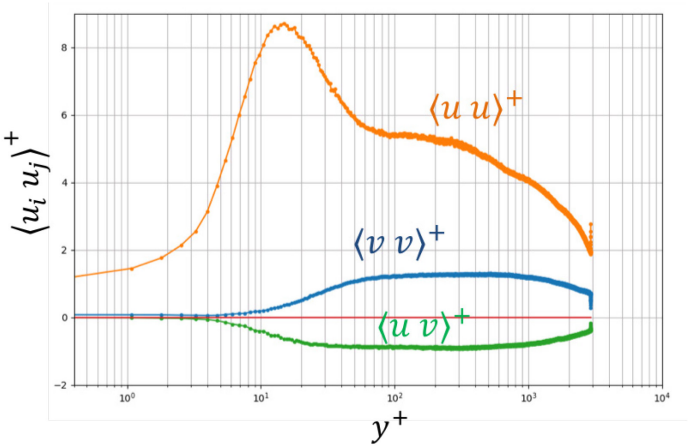

Fig. 16: Variances and co-variance of the stream-wise and wall-normal velocity components with inner scaling (from [14])

3.2. Measurement of free shear flows

Beyond boundary layer characterization the described PIV approach is also well suited for the measurement of a variety of other turbulent flows such as free jets or shear layers. The setup shown in Fig. 17, left, was operated at image frame rates up to 420 kHz to demonstrate the possibility of capturing high speed velocity data O(100 m/s) at image magnifications near unity using a moderately powered high-speed laser (Innolas Photonics, Nanio-Air) that has an integral power of 10W at the design frequency of 40 kHz. The sample snap shot of a sequence acquired at 250 kHz is shown in Fig. 17, middle, and was acquired with an iX-Cameras iSpeed 720 high speed camera, providing a field of view of 676×72 pixel at a magnification of 13.8 µm per pixel. Fig. 17, right, shows an exemplary power spectrum that can be obtained from the acquired high-speed PIV data and was computed from a sequence consisting of 840,000 images (64×96 pixels).

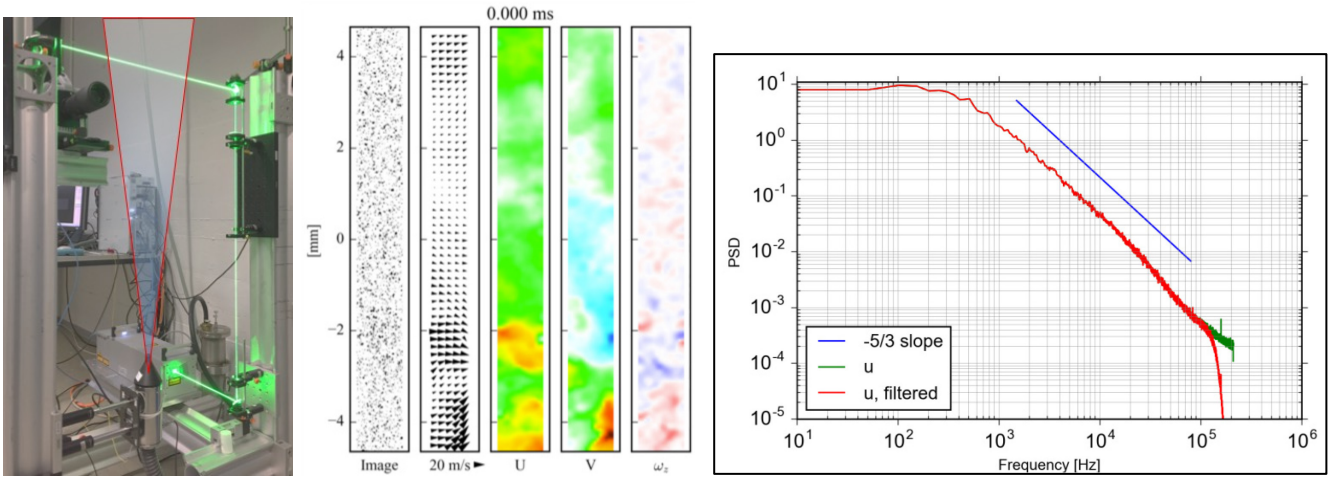

Fig. 17: Left: measurement setup on a free jet, middle: single data set of a free jet on the centerline acquired at x/D=15 and 250 kHz sample rate for a Reynolds number of Re_D = 93,000; right: spectrum of the streamwise velocity acquired at 420 kHz for a Reynolds number of Re_D = 120,000

3.3. “Profile-PIV” Measurements inside a diffusor

Within the DLR project VicToria the “profile PIV” technique was extensively used to get converged velocity statistics of the flow inside a small divergent channel. The project is motivated by improving the turbulence models used in RANS-based CFD on the basis of experimental validation data, in particular, for wall bounded flows subjected to adverse pressure gradient close to flow separation. A photograph small-scale wind tunnel is shown in Fig. 18, left. On the entry side the duct has a square cross section of 76×76 mm^2 followed by two-fold area increase within a streamwise distance of 6H (456 mm). A settling chamber and 10:1 contraction upstream of the duct provided uniform inflow conditions. A grid immediately upstream of the duct introduced free stream turbulence of about 2% at the start of the diffuser ramp. Using variable speed suction blowers, the bulk velocity at the inlet was adjusted to U_{in} = 10m/s (Re_H = 51,000). The entire tunnel could be traversed in a horizontal plane such that image data could be acquired at many locations with minimal adjustments to the camera-laser setup, thereby allowing a near automated data acquisition.

For the “profile-PIV” a scientific CMOS camera (PCO Edge5.5) was used in place of the normally used high-speed camera. By reducing the field of view to 2560(W)×200(H) this camera could provide double-frame rates exceeding 200 Hz such that 10,000 statistically independent samples could be acquired within one minute. Overall more than 100 locations were sampled in this way. For each position the subsequent, automated PIV processing provided the relevant profiles of velocity and associated moments and estimates of the mean and unsteady stream-wise wall shear stress. An example of measured profiles and accompanying RANS prediction is provided in Fig. 18, right. The wall-shear rate (du/dy), obtained by the near-wall processing scheme described in Section 3.1.2, was used to estimate the skin friction coefficients at each measurement location. A comparison between the measured and computed skin friction distribution is provided in Fig. 19. While the values for the flat wall opposite of the ramp (Fig. 19, left) match quite well, even among the different RANS models, the skin friction along the ramp shows higher discrepancies between experiment and simulation, especially toward in the off-center planes toward the side wall (Fig. 19, right). This can be explained by the

underestimation of strong corner separation zones by all RANS models in comparison to flow field data acquired with conventional stereo-PIV.

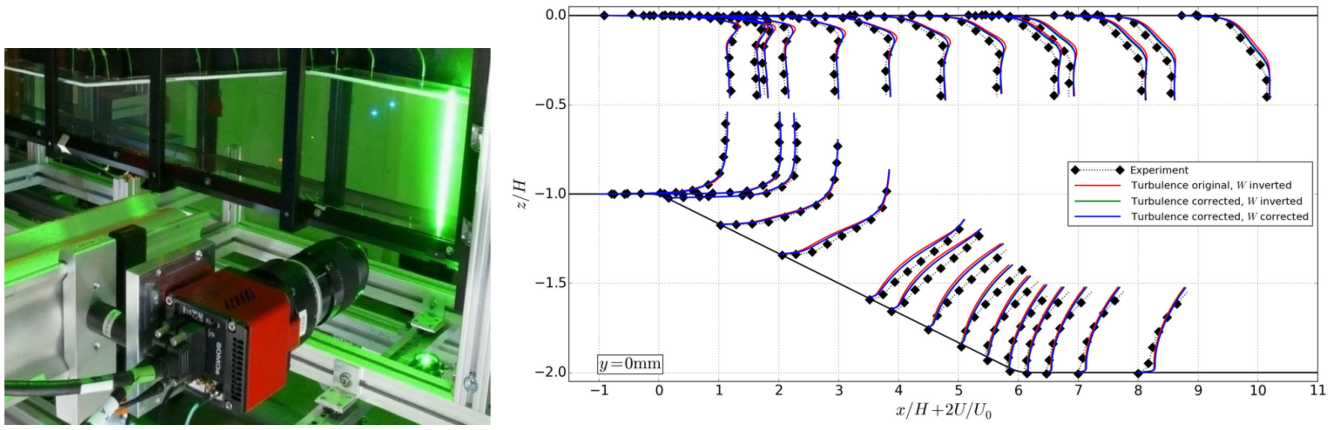

Fig. 18: Left: small rectangular channel with diffusor on traversing frame with profile imaging setup using sCMOS camera operated at a double frame rate of 200 Hz. Right: velocity profiles acquired on the centerline compared with results from numerical simulation

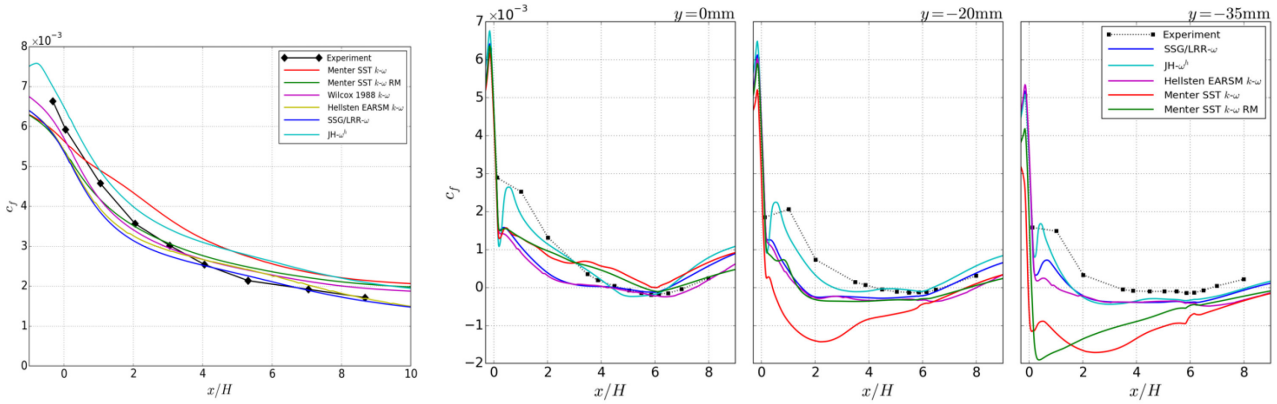

Fig. 19: Measured skin friction coefficients for the flat wall (left-most) and diffuser wall (right) at different span-wise locations in comparison to results obtained with RANS simulations

4. Summary and outlook

The article presented the development, working principles and application examples of a variant of the well-established PIV technique that is particularly suited in providing converged statistics of turbulent flows as well as spectra and correlations of the acquired velocity components. The use of high aspect ratio image formats on state-of-the-art cameras nowadays allows sample counts in the order 10^5 up to 10^6 at frame rates of similar magnitudes. The continuous development of high-speed imaging and high-speed lasers will extend these limits even further. Advanced particle image processing schemes such as the recently introduced multi-frame "shake-the-box" PTV scheme allows to retrieve flow velocity information with significantly improved error bounds in comparison to the commonly used two-frame based analysis schemes. However, it should be pointed out that with increasing flow velocity and associated higher velocity gradients, the actual signal bearer – the tracer particle – will show an increasing degree of velocity lag, acting as a low-pass filter while subjected to external flow forces and needs to be taken into account when utilizing the measured data.

References

[1] Adrian R, Westerweel J (2011): Particle Image Velocimetry. Cambridge University Press, Cambridge (UK), ISBN 978-0521440080

[2] Alfredsson PH, Johansson AV, Haritonidis JH, Eckelmann H (1988). The fluctuating wall-shear stress and the velocity field in the viscous sublayer. *Physics of Fluids* 31(5), 1026–9. http://doi.org/10.1063/1.866783

[3] Becker, K.; Heitkamp, K. & Kügeler, E. (2010) Recent Progress In A Hybrid-Grid CFD Solver For Turbomachinery Flows, 5th European Conference on Computational Fluid Dynamics, ECCOMAS CFD 2010, 2010

[4] Cuvier C, Srinath S, Stanislas M, Foucaut JM, Laval JP, Kähler CJ, et al. (2017). Extensive characterisation of a high Reynolds number decelerating boundary layer using advanced optical metrology. *Journal of Turbulence*, 18(10), 929-972. http://doi.org/10.1080/14685248.2017.1342827

[5] Diaz-Daniel C, Laizet S, Vassilicos JC (2017): Wall shear stress fluctuations: Mixed scaling and their effects on velocity fluctuations in a turbulent boundary layer. *Physics of Fluids* 29(5), 055102–15. http://doi.org/10.1063/1.4984002

[6] Elsinga GE, Scarano F, Wieneke B, van Oudheusden BW (2006): Tomographic Particle Image Velocimetry. *Exp. Fluids* 41: 933. https://doi.org/10.1007/s00348-006-0212-z

[7] Hergt A, Steinert W, Grund S (2013): Design and Experimental Investigation of a Compressor Cascade for Low Reynolds Number Conditions. 21st International Symposium on Air Breathing Engines (ISABE), 09-13 Sep. 2013, Busan, Korea

[8] Klinner J (2017): *Development and assessment of volume resolving velocimetry for turbomachinery test facilities.* Dissertation. DLR-Research Report. DLR-FB-2017-52. https://elib.dlr.de/117111/

[9] Örlü R, Schlatter P (2011): On the fluctuating wall-shear stress in zero pressure-gradient turbulent boundary layer flows. *Physics of Fluids* 23(2), 021704–5. http://doi.org/10.1063/1.3555191

[10] Raffel M, Willert C, Scarano F, Kähler C, Wereley S, Kompenhans J (2018) Particle Image Velocimetry – A Practical Guide, 3rd Edition, Springer International Publishing AG, ISBN 978-3-319-68852-7

[11] Schanz D, Gesemann S, Schröder A (2016): Shake-The-Box: Lagrangian particle tracking at high particle image densities. *Experiments in Fluids* 57(5), 1-27. http://doi.org/10.1007/s00348-016-2157-1

[12] Schanz D, Geisler R, Jahn T, Schröder A, Cornic P, Leclaire B, Gallas Q (2017) Volumetric characterization of the flow around a cubical obstacle. 12th International Symposium on Particle Image Velocimetry (ISPIV 2017), 18-22 June 2017, Busan, Korea.

[13] Schröder A, Schanz D, Geisler R, Novara M, Willert C (2015) Near-wall turbulence characterization using 4D-PTV "Shake-The-Box". 11th International Symposium on Particle Image Velocimetry (PIV2015), 14-16 Sep. 2015, Santa Barbara (CA), USA

[14] Schröder A, Schanz D, Novara M, Philipp F, Geisler R, Agocs J, Knopp T, Schroll M, Willert CE (2018) Investigation of a high Reynolds number turbulent boundary layer flow with adverse pressure gradients using PIV and 2D- and 3D- Shake-The-Box. 19th International Symposium on Laser and Imaging Techniques to Fluid Mechanics, 16-19 July 2018, Lisbon, Portugal

[15] Thais L, Tejada-Martínez AE, Gatski TB, Mompean G, (2011) A massively parallel hybrid scheme for direct numerical simulation of turbulent viscoelastic channel flow. Computers & Fluids 43(1): 134-142. https://doi.org/10.1016/j.compfluid.2010.09.025.

[16] Wieneke B (2013) Iterative reconstruction of volumetric particle distribution. Meas Sci Technol 24:024008. https://doi.org/10.1088/0957-0233/24/2/024008

[17] Willert CE (2015): High-speed particle image velocimetry for the efficient measurement of turbulence statistics. Experiments in Fluids 56(1), 17. http://doi.org/10.1007/s00348-014-1892-4

[18] Willert CE, Soria J, Stanislas M, Klinner J, Amili O, Eisfelder M, et al. (2017): Near-wall statistics of a turbulent pipe flow at shear Reynolds numbers up to 40 000. Journal of Fluid Mechanics, 826, R5. http://doi.org/10.1017/jfm.2017.498

[19] Willert CE, Cuvier C, Foucaut JM, Klinner J, Stanislas M, Laval JP, et al. (2018): Experimental evidence of near-wall reverse flow events in a zero pressure gradient turbulent boundary layer. Experimental Thermal and Fluid Science, 91, 320–328. http://doi.org/10.1016/j.expthermflusci.2017.10.033

[20] Willert CE, Soria J, Cuvier C, Foucaut JM, Laval JP (2018): Flow reversal in turbulent boundary layers with varying pressure gradients. 19th International Symposium on Laser and Imaging Techniques to Fluid Mechanics, 16-19 July 2018, Lisbon, Portugal. https://elib.dlr.de/121145/

Acknowledgment

The author is indebted to a considerable number of colleagues, partner institutions and friends that made not only development the technique possible but also resulted in a number of applications at a variety of facilities. The support of the EuHIT Framework 7 EC project (European High-Performance Infrastructures in Turbulence, http://www.EUHIT.org , grant agreement no: 312778) for the financial support which has allowed be the measurements at LMFL in May 2015 as well as at the CICLoPE long pipe facility of the Univ. of Bologna in May 2016. Subsequent measurements of the near wall velocity statistics at LMFL in November 2017 were made possible through the financial support of the university Centrale Lille.

Copyright Statement